ELSEVIER

Atmospheric Environment 38 (2004) 993–1003

ATMOSPHERIC ENVIRONMENT

www.elsevier.com/locate/atmosenv

Precipitation scavenging of atmospheric aerosols for emergency response applications: testing an updated model with new real-time data

Gwen A. Loosmore*, Richard T. Cederwall

Atmospheric Science Division, Lawrence Livermore National Laboratory, P.O. Box 808, L-103, Livermore, CA 94551, USA

Received 17 August 2003; accepted 26 October 2003

Abstract

Precipitation scavenging can effectively remove particulates from the atmosphere. Interest in the phenomena waxed in the 1980s, but models developed at that time remain limited by the lack of both detailed, time-resolved wet deposition pattern measurements for model confirmation and real-time rain data for model execution. Recently, new rain products have become available that can revolutionize real-time use of precipitation scavenging models on the regional scale. We have utilized a 4-km, hourly resolution precipitation data set from the Arkansas Red-Basin River Forecast Center. A standard below-cloud aerosol scavenging model has been modified to incorporate the potentially larger scavenging in heavy rain events. This paper demonstrates the model on a sample rainfall data set. The simulations demonstrate the concentrating effect of rainfall, especially heavy rain, on deposition patterns. Wet deposition played an important role in the simulated fate and transport, removing as much as 70% of the released aerosol.

Keywords: Wet deposition; Aerosol; Modeling; Particle; Washout

1. Introduction

Precipitation scavenging is the removal of material from the atmosphere by hydrometeors. Precipitation scavenging goes by several different names, including wet deposition, rainout (typically used for in-cloud processes), and washout (typically used for below-cloud processes). The work described here focuses on the scavenging of aerosol particles by raindrops. Precipitation scavenging has been shown to effectively remove pollutants from the atmosphere. For example, after the Chernobyl event, significant radioactivity was wet deposited in Northern Europe (Jylha, 1991). Wet deposition velocities are typically much larger than dry deposition velocities (Slinn, 1984). Thus precipitation scavenging should be included in real-time modeling of atmospheric transport for hazardous materials. However, modeling of precipitation scavenging has been limited by access to real-time rain data. Recent work by the National Center for Environmental Prediction (NCEP) is changing this scenario. The NCEP is producing an hourly Stage IV precipitation product on a 4 km grid that incorporates multi-sensor (gauge + WSR-88D radar) precipitation data from across the continental United States (NCEP, 2003). The radar data is bias-adjusted using the gauge data, which are assumed to be ground truth; the gauge data are then used to complete the precipitation product where radar data are inadequate (Lawrence et al., 2003; Seo et al., 1999). We used such a multi-sensor precipitation data set to test a new precipitation scavenging model developed for emergency release scenarios at the Department of Energy's National Atmospheric Release Advisory Center (NARAC) at Lawrence Livermore National

*Corresponding author. Tel.: +1-925-423-0214; fax: +1-925-422-5844.

E-mail address: loosmorel@llnl.gov (G.A. Loosmore).

1352-2310/$ - see front matter © 2003 Elsevier Ltd. All rights reserved.
doi:10.1016/j.atmosenv.2003.10.055

Nomenclature

List of symbols

d_p	aerosol particle aerodynamic diameter
k	Boltzmann constant
v_s	gravitational settling velocity of a particle
C_c	Cunningham correction factor
D	raindrop diameter
D_B	particle Brownian diffusivity
D_r	representative raindrop diameter
E	efficiency of capture
J	rain rate (mm h^{-1})
M	mass or activity of Lagrangian particle
N	number density of droplets
Re	raindrop Reynolds number (for radius)
Sc	aerosol particle Schmidt number
St	Stokes number
S_*	critical Stokes number for impaction
T	temperature in degrees Kelvin
V	terminal settling velocity of raindrop
ϕ	diameter ratio (d_p/D)
λ	scavenging coefficient
ρ_a	air density
ρ_p	particle density
ρ_w	water density
μ_a	air viscosity
μ_w	water viscosity
ν	kinematic viscosity
ν_s	particle gravitational settling velocity
τ	particle relaxation time
ω	viscosity ratio (μ_w/μ_a)

Laboratory. The NARAC system provides both real-time operational predictions and detailed assessments for atmospheric releases of hazardous materials.

This paper (1) describes and demonstrates the new scavenging model using rainfall data, (2) explores the sensitivity of wet deposition to particle size, and (3) compares the importance of wet and dry deposition. The results presented here are simulations of regional wet deposition patterns. As such, they are not contrasted with empirical data sets, as there are no appropriate data for comparison. Previous field studies, such as PRE-STORM (Cunning, 1986) and PRECP (Daum et al., 1990) have used a coarse array of surface sampling in conjunction with in situ airborne sampling; these data sets are too coarse to match the simulation. Scavenging coefficients predicted with the present model are consistent with data from previous experiments (Andronache, 2003; Slinn, 1984).

2. The new precipitation scavenging model

2.1. Background/context

These development efforts are intended to enhance capabilities of the NARAC system. NARAC utilizes a Lagrangian particle dispersion model, LODI (Nasstrom et al., 2000) which is driven by forecast or observational meteorological data. The precipitation scavenging algorithm has been designed for use in real-time modeling of accidental releases of hazardous material in the boundary layer. In the general case, simulations can draw on rain rates and limited other meteorological data, but no information about cloud formation or structure will be available.

Although state-of-the-art, the NCEP precipitation data are limited; there will generally not be data on cloud base location or whether a system is convective. The 4 km spatial (linear) resolution and the 1 h temporal resolution are insufficient to resolve local storm cells and edges. Within a convective system, updrafts may bring aerosol particles into the cloud, where some fraction may serve as cloud condensation nuclei (CCN), grow quickly to droplets, and fall as rain. It may be possible to infer from a heavy rain rate that the system is convective, but there will not be data on the updraft velocities. Nor will there be information about the vertical profile of rain (indicating virga, for example). There is insufficient input data for simulating cloud microphysics. Nor can the cloud parameterizations in GCMs appropriate for larger grids be directly adopted in regional simulations. The precipitation scavenging algorithm, therefore, must rely on the rain rate alone. Furthermore, the computational expense of the precipitation scavenging algorithm must be commensurate with its importance in the overall context of the fate-and-transport simulation.

2.2. Mathematical description of below-cloud precipitation scavenging

The work in this paper builds on Slinn's (1984) semi-empirical formulation for below-cloud scavenging, which continues to be used for contemporary studies (Chate et al., 2003). The mechanisms of aerosol scavenging by rain have been reviewed elsewhere (Slinn, 1984) and will be described only briefly here. We incorporate a few recent results to devise a robust algorithm for real-time emergency response applications. Wet-deposition is modeled using a first-order decay equation, where M represents the mass or activity of a Lagrangian particle of diameter d_p, and λ is the scavenging coefficient:

$$\dot{M} = -\lambda M. \tag{1}$$

The scavenging coefficient, λ, is the integral over all raindrop diameters D:

$$\lambda(d_p) = \int_0^\infty \frac{\pi}{4} D^2 V(D) E(D, d_p) N(D)\, dD. \quad (2)$$

Here d_p is the aerosol diameter, V is the raindrop fall velocity, N is the raindrop size distribution function, and E is the capture efficiency.

Two factors contribute to λ: (1) the fractional area swept by the falling raindrops is a complicated function of the raindrop size distribution, incorporating the effect of the surface-to-volume ratio; (2) the capture efficiency E represents the fraction of aerosol particles in the raindrop sweep volume that are actually captured. Here a collision is assumed to result in perfect sticking; in reality, aerosol particles may bounce off a raindrop, if the interfacial conditions (beyond the scope of this paper) so dictate.

Slinn's (1984) "semi-empirical" model for the capture efficiency E incorporates the effects of Stokes and Reynolds number considerations, including Brownian diffusion across streamlines:

$$E = \frac{4}{Re\, Sc}[1 + 0.4 Re^{1/2} Sc^{1/3} + 0.16 Re^{1/2} Sc^{1/2}] + 4\phi[\omega^{-1} + (1 + 2Re^{0.5})\phi] + \left[\frac{St - S_*}{St - S_* + 2/3}\right]^{3/2} \left(\frac{\rho_p}{\rho_w}\right)^{1/2}, \quad (3)$$

where

$$Re = \frac{DV\rho_a}{2\mu_a}, \quad Sc = \frac{\mu_a}{\rho_a D_B}, \quad D_B = \frac{kTC_c}{3\pi\mu_a d_p},$$
$$\tau = \frac{(\rho_p - \rho_a) d_p^2 C_c}{18\mu_a}, \quad St = \frac{2\tau(V - v_s)}{D},$$
$$\omega = \frac{\mu_w}{\mu_a}, \quad \phi = \frac{d_p}{D}, \quad S^* = \frac{1.2 + \frac{1}{12}\ln(1 + Re)}{1 + \ln(1 + Re)}. \quad (4)$$

Symbols are defined on the previous page. This model captures the relationship between a larger sphere (the raindrop) falling toward a smaller sphere (the aerosol particle); if the particle follows the fluid streamlines past the raindrop it may still be captured by Brownian diffusion or interception, otherwise it is susceptible to direct interception through collision. The first term in Eq. (3) represents Brownian diffusion, the second interception, and the third impaction. Phoretic forces have been neglected; Carstens and Martin (1982) calculate the effect of phoretic forces to be offset by the decrease in drop lifetime.

Brownian diffusion becomes increasingly important with shrinking particle size. Impaction, by contrast, can only occur for particles with Stokes numbers above the critical value of 1.2 (Phillips and Kaye, 1999; Slinn, 1974), hence this term is not included for unit-density particles smaller than about 3 μm. Interception is the least important of the three terms. This creates a range of particles with small Brownian diffusivities and low Stokes numbers, resulting in a minimum (for particles near 1 μm in diameter) in the scavenging coefficient curve (presented in Fig. 1, which is discussed below). This minimum is typically called the "Greenfield gap" after Greenfield, who first identified this feature (Greenfield, 1957). By contrast, we note that the model of Horn et al. (1988) neglects the critical Stokes number for impaction and thus overestimates the collection efficiency in the Greenfield gap (Sparmacher et al., 1993). The integral form for the scavenging coefficient is simplified using a representative size D_r (Seinfeld and Pandis, 1998):

$$\lambda(d_p) = \frac{\pi}{4} D_r^2 V(D_r) E(D_r, d_p) N(D_r). \quad (5)$$

Expressing the rain rate J (mm h^{-1}) as:

$$J = \int_0^\infty \frac{\pi}{6} D^3 V(D) N(D)\, dD = \frac{\pi}{6} D_r^3 V(D_r) N(D_r) \quad (6)$$

and

$$\lambda(d_p) = \frac{3}{2} \frac{E(D_r, d_p)}{D_r} J. \quad (7)$$

Collection efficiency decreases with raindrop size. The ideal D_r would effectively represent the collection efficiency for the full range of raindrop diameters in any given storm, blending the higher efficiency of the smaller raindrops with the lesser efficiency of the larger. In other words, the overall scavenging coefficient calculated with D_r ideally would match that computed from the full integral over raindrop sizes (from Eq. (2)). We adopt the median volume diameter for a gamma

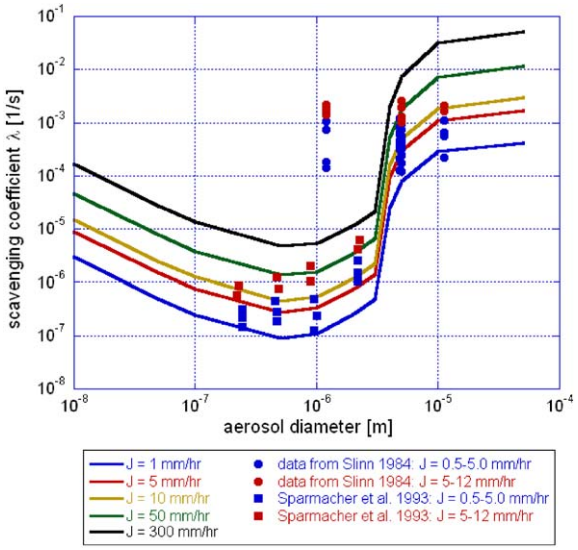

Fig. 1. Scavenging coefficients as a function of particle size and rain rate.

raindrop size distribution (Willis, 1984) for D_r (mm):

$$D_r = 0.97J^{0.158}. \quad (8)$$

With this formulation, D_r ranges from ~1 to 2 mm. The scavenging coefficient, λ (h^{-1}) is thus computed from:

$$\lambda(d_p) = 1.546EJ^{0.842}. \quad (9)$$

We use an empirical fit for the raindrop terminal velocity in the calculations (Willis, 1984):

$$V = 4854D_r \exp(-195D_r). \quad (10)$$

Nieto et al. (1994) compute scavenging coefficients directly from raindrop size distributions without adopting a representative diameter D_r. Scavenging coefficients presented in that paper are indistinguishable from those computed with Eq. (9), above. For this reason, it is expected that uncertainties in the aerosol particle source term will play a larger role in the overall precipitation scavenging uncertainty than does the use of a representative diameter. However, it is important to recognize the additional implicit assumptions that have been made here. The representative raindrop size is assumed to apply at all heights, as is the terminal velocity formulation despite being derived from measurements made at the earth's surface (Pruppacher and Klett, 1980). The difference in swept area for distributions with many small drops is blurred, compared with a larger distribution. No effort is made to parameterize fluctuations in the distribution resulting from self-coagulation, evaporation, or other processes. Nonetheless, scavenging coefficients generated with this model are consistent with those generated from raindrop distributions and observed data (Andronache, 2003; Slinn, 1984).

Values of the scavenging coefficient λ, for a range of rain rates, are plotted versus aerosol particle diameter in Fig. 1. The scavenging coefficient spans orders of magnitude over the aerosol sizes of interest, primarily reflective of the variation in efficiencies over that range. Also plotted are two sets of data, from Slinn (1984) and from Sparmacher et al. (1993), evocative of the true uncertainty in below-cloud scavenging. The model presented here is mildly conservative with respect to the Sparmacher data and decidedly conservative with respect to data presented in Slinn, for which the Greenfield gap (the minimum for micron-sized particles) is apparently bridged.

Theoretically, the model developed above is likely to underestimate precipitation scavenging, especially at high rain rates. The above model includes only a subset of the mechanisms that influence collisions, neglecting thermo- and diffusiophoresis, turbulence, and charging effects. Furthermore, the algorithm was intended for below-cloud processing. In convective systems, or for high-altitude releases, aerosol particles may be drawn up into the cloud. For these reasons, operationally it may be appropriate to increase precipitation scavenging for these events. In the general case, the model meteorological inputs will include only the hourly, 4 km rain rate and associated wind fields. Without further information about cloud base, updraft strength, etc., it is impossible to directly simulate the aerosol particle participation in in-cloud processes. Nor would it be appropriate to expend computational resources in these calculations. Instead, the entire system must be parameterized. To this end, the following optional heavy rain algorithm was devised: when a unit-density aerosol particle greater than or equal to 0.2 μm in diameter encounters a rain rate greater than or equal to 25 mm h^{-1}, it is treated as a 10 μm particle and scavenged at the appropriate below-cloud rate for that timestep:

IF($J \geqslant 25.0$) THEN
IF($2.0 \times 10^{-7} \leqslant d_p \leqslant 1.0 \times 10^{-5}$) THEN
$d_p\_heavy = 1.0 \times 10^{-5}$
ELSE
$d_p\_heavy = d_p$
END IF
END IF

(and use d_p_heavy to compute λ for this part of the timestep). This is consistent with Slinn's data as presented in Fig. 1, which show scavenging rates for micron-sized particles as large as those predicted for 10 μm particles. This algorithm will have a dramatic effect on the scavenging coefficient for particles smaller than about 3 μm, as is evident from Fig. 1. These small particles have below-cloud scavenging coefficients that are orders of magnitude smaller than the scavenging coefficients for 10 μm particles, at a given rain rate. The heavy-rain algorithm is therefore not an enhancement of the below-cloud algorithm but an entirely different regime, reflective of the very-effective in-cloud scavenging that may occur. In-cloud scavenging can also occur at significant rates for non-convective scenarios and lower precipitation rates, but convective scenarios also provide a means for aerosols to be drawn in-cloud.

The rain-rate cutoff of 25 mm h^{-1} was chosen to be representative of a convective situation (Chin, 1994; Rogers and Zawadzki, 1979) in which strong updrafts could move aerosol particles into clouds to provide opportunities for nucleation scavenging. Because in-cloud scavenging can occur at precipitation rates smaller than 25 mm h^{-1}, the cutoff is adjustable. The value of 0.2 μm was chosen as a lower bound for which particles will effectively serve as CCN (Flossmann, 1985; Seinfeld and Pandis, 1998). Ten microns are intended as a logical small droplet size for nucleated particles. The timescales of uptake, nucleation, and droplet growth have not been treated explicitly; the assumption is made that for the regional grids of interest (spanning a few km per cell),

Table 1
List of simulations executed

Simulation name	Mass median diameter (m)	Precipitation scavenging algorithm	Wet deposition computed?	Dry deposition computed?
big_std	10^{-5}	Standard below-cloud	Yes	Yes
big_hr	10^{-5}	heavy_rain	Yes	Yes
big_norain	10^{-5}	None	No	Yes
small_std	10^{-6}	standard below-cloud	Yes	Yes
small_hr	10^{-6}	heavy_rain	Yes	Yes
small_norain	10^{-6}	None	No	Yes

there is sufficient time for the processes to occur before the particle would advect across gridlines. Thus, the model would not be appropriate for urban-scale grids (spanning meters to tens of meters per cell).

3. Description of simulations

The test simulations used data from an inhomogeneous precipitation event crossing through north-central Oklahoma and south-central Kansas on 18 July 1997. Observed meteorological data from the DOE Atmospheric Radiation Measurement Program provided the near-surface winds every 30 min and vertical profiles of winds every 3 h. The 4-km, hourly precipitation data set was computed at the Arkansas Red-Basin River Forecast Center, using reflectivity from numerous weather radars and observed precipitation from over 100 rain gauges.

Simulations were executed on a 4 km grid; rain rates were interpolated from the grid to the Lagrangian particle locations at each timestep. The simulated contaminant source emitted continuously in the southeast corner of the domain, at 10 m height, at a location expected to be buffeted by the storm. A total of 200,000 particles were used for the 15-h release. A post-processor smoothing algorithm (1:2:1 filter) was used to smooth anomalies introduced by discrete particles. For reasons not related to this paper, the source term emitted CS-137 at a rate equivalent to that in the first day of the Chernobyl accident (Gudiksen and Lange, 1986). Decay of CS-137 (1/2 life of 30.17 years) was negligible over the time of the simulation. For the purposes of illustration, the cesium serves as a surrogate for any aerosol with a similar aerodynamic size distribution.

A total of six simulations were conducted. Two different lognormal distributions were used for the emitted cesium aerosol, both with a minimum diameter of 1.0×10^{-7} m and a maximum of 5.0×10^{-5} m, but with mass median diameters (mmd) of 1.0×10^{-5} and 1.0×10^{-6} m. Simulations were conducted with the heavy rain algorithm on and off; and with and without rain included. In the discussion below, these simulations are called *big_std* (bigger mmd, standard below-cloud algorithm), *big_hr* (bigger mmd, heavy rain algorithm on), and similarly, *small_std*, and *small_hr*. Identical simulations without rain are entitled *small_norain* and *big_norain*. Table 1 lists the simulations and their properties. These six simulations present ten possible deposition fields, which are analyzed and described in the text below, and presented (normalized, as below) in Fig. 6. The difference between the big and small particle size distributions can be seen in Fig. 2. Of particular interest is the mass fraction smaller than 2×10^{-7} μm, which is exempt from heavy rain scavenging; this fraction constitutes approximately 8% of the small and only 0.02% of the big distribution. The motivation for these six simulations is to investigate the relative importance of wet and dry deposition, not only within rain events, but also in the absence of rain. The effect of particle size is expected to be important from the shape of the scavenging curve. Finally, there is interest in examining the impact of the heavy rain algorithm for an appropriately heavy rain event.

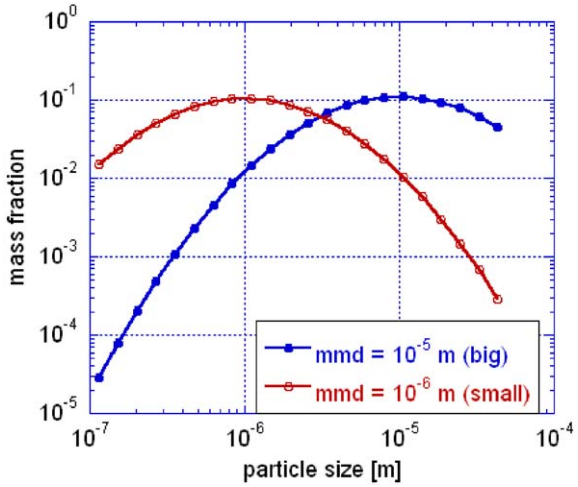

Fig. 2. Particle size distributions used in the simulations.

4. Results

4.1. Precipitation rates on plume

Fig. 3 shows the gridded precipitation rates encountered by the plume over time. A no-rain hourly average air concentration plume was used to generate this subset of the precipitation data; the plotted precipitation rates represent the gridded rain rates that would have affected that plume, at that time of the simulation, had the rain been included. Because gridded rain rates represent average rain values from the preceding hour, the precipitation data for hour $n+1$ were used in the calculations from hour n to hour $n+1$. In the figure, hour 2 therefore represents the precipitation used for the second simulated hour. There was no rain encountered in the first hour.

The first heavy rain on the plume ($\geqslant 25\,\mathrm{mm\,h^{-1}}$) appears in hour 4, and the plume continues to encounter heavy rain through hour 10 (solid lines). Hour 7 appears to be the heaviest part of the storm, with nearly 15% of the gridded precipitation rates sampled by the plume exceeding $25\,\mathrm{mm\,h^{-1}}$. Note that the rain rates used for the scavenging calculation for a given Lagrangian particle are bilinearly interpolated from the grid to the particle position, so the presence of a gridded rain rate $>25\,\mathrm{mm\,h^{-1}}$ does not ensure that the heavy rain algorithm is utilized.

The approximate fraction of the plume that is encountering rain, as a function of time, is shown in Fig. 4a. This fraction increases steadily to hour 4, then drops, both because the rain is highly localized, and because the plume continues to grow. The smallest plume coverage is seen concurrent with the heaviest rain, at hour 7. By hours 9 and past, the rain covers much of the extended plume area. These fluctuations in rained-on plume fraction are reflected in the deposition areas, as explained below. To give a sense of the shape of the storm, Fig. 4b shows snapshots of the precipitation (in blue), including an approximate plume outline (in red) at hours 7 and 9. Darker blue contours indicate heavier precipitation rates, and the wind directions at 10 m are shown with arrows.

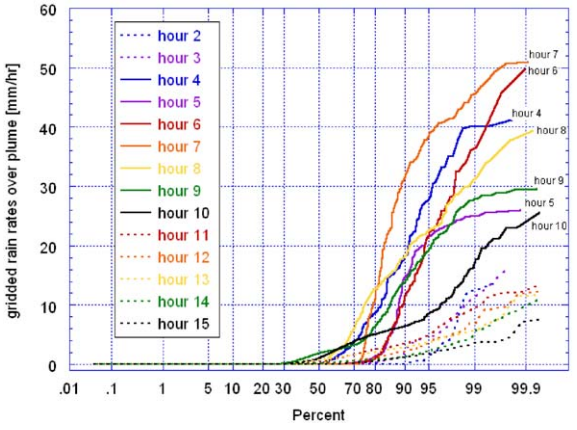

Fig. 3. Cumulative distributions for rain encountered by plume.

Fig. 5 shows snapshots of the simulated wet deposition at hour 15, to indicate the concentrating effect of the heavy rain algorithm and the inhomogeneous hot spots that may occur with wet deposition events in with time- and spatially varying precipitation. The contours use levels of 160, 1.6×10^{4}, 1.6×10^{5}, 1×10^{7}, and $1\times10^{9}\,\mathrm{Bq\,m^{-2}}$, thus the colors represent the following ranges: yellow—below action level; light orange—from action level to 10 times greater; dark orange—from 10 to 625 times above action level, and red—up to 6.25×10^{4} times the action level. The precise location is left unidentified for national security reasons.

4.2. Mass deposited and area covered

Fig. 6 contrasts the deposited mass and areas of the depositions for the six simulations, treating dry and wet deposition separately. Wet deposition fields are shown in blue, with lighter blue representing the standard algorithm and dark blue the heavy rain. Dry deposition fields are shown in warm tones, with red representing the no-rain simulations, brown the heavy rain, and orange the standard algorithm. Smaller symbols represent the small mmd. While there were six simulations, two (the no-rain cases) have only dry deposition fields.

The results in Fig. 6 are consistent with expectations. Precipitation scavenging is most effective for the big mmd, and with the heavy rain algorithm on. Heavy rain creates deposition hot spots, reflective of the locally heavy rain that triggers the algorithm. This concentration has two effects: locally higher deposition values, and smaller deposition values outside the concentrated areas, when contrasted with the standard algorithm. The small mmd, with more particles in the Greenfield gap, is much more poorly scavenged by the standard algorithm than is the big mmd.

The (wet and dry) deposited mass for the various simulations are plotted in Fig. 6a as mass fractions, i.e. as the deposited mass normalized by the total emitted mass (up to that time of the simulation). In other words, at hour 4, roughly 50% of the total mass emitted in the first four hours was wet deposited in the big_hr simulation. Deposition plays an important role in determining the fate of the aerosol. From hour 4 on, 60–80% of the big mmd is deposited (wet and dry) when rain is included, most of that by wet deposition. With the standard algorithm, about 20% of the smaller size aerosol material (small mmd) is deposited, with wet and dry deposition contributing about equally. With the heavy rain algorithm, for the small mmd, the wet

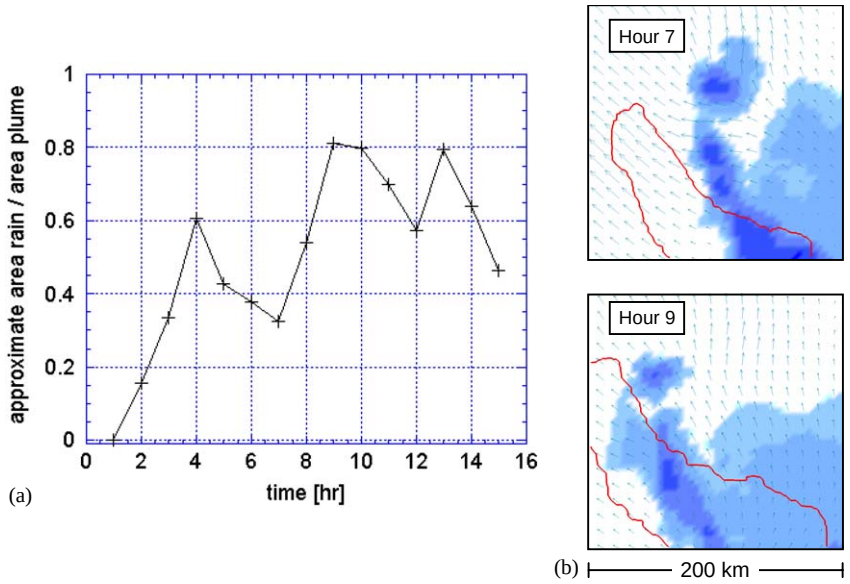

Fig. 4. (a) Fraction of horizontal extent of simulated aerosol plume that overlaps non-zero gridded rain; and (b) snapshots of the storm at hours 7 and 9, with plume outline shown.

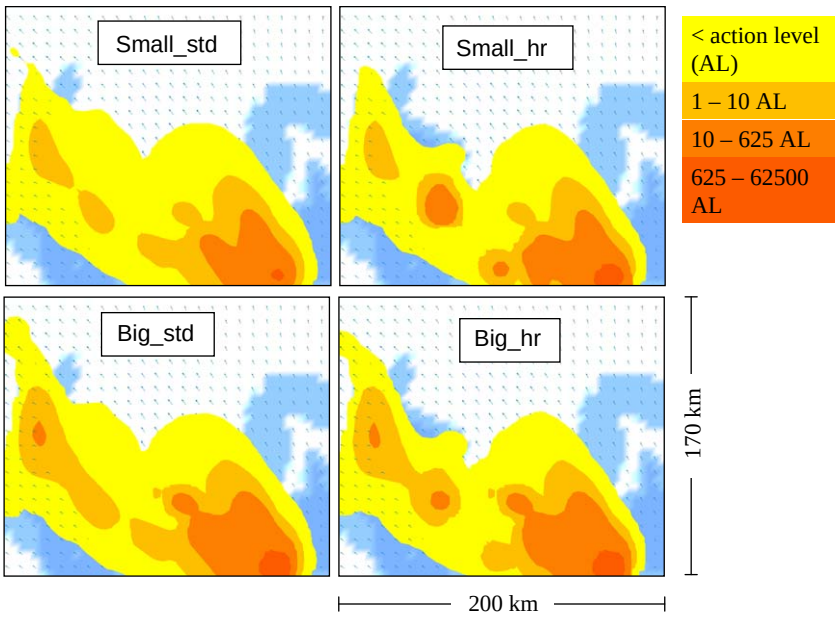

Fig. 5. The wet deposition fields at hour 15 of the simulation.

deposition increases markedly, jumping as high as ~48% at hour 7 (almost 5 times the dry deposition), and falling to roughly 30% by the end of the simulation (still a factor of 3 greater than dry deposition). By contrast, dry deposition alone (simulations without rain) accounts for only 20–30% of the material with the big mmd and <10% for the small mmd.

Dry deposition and wet deposition are not completely independent: the more effectively material is wet deposited, the less material is available to dry deposit. The larger particles are most effectively scavenged by rain, and these also have the largest dry deposition velocities. Thus, when less wet deposition occurs, more particles are available to be dry deposited. Thus,

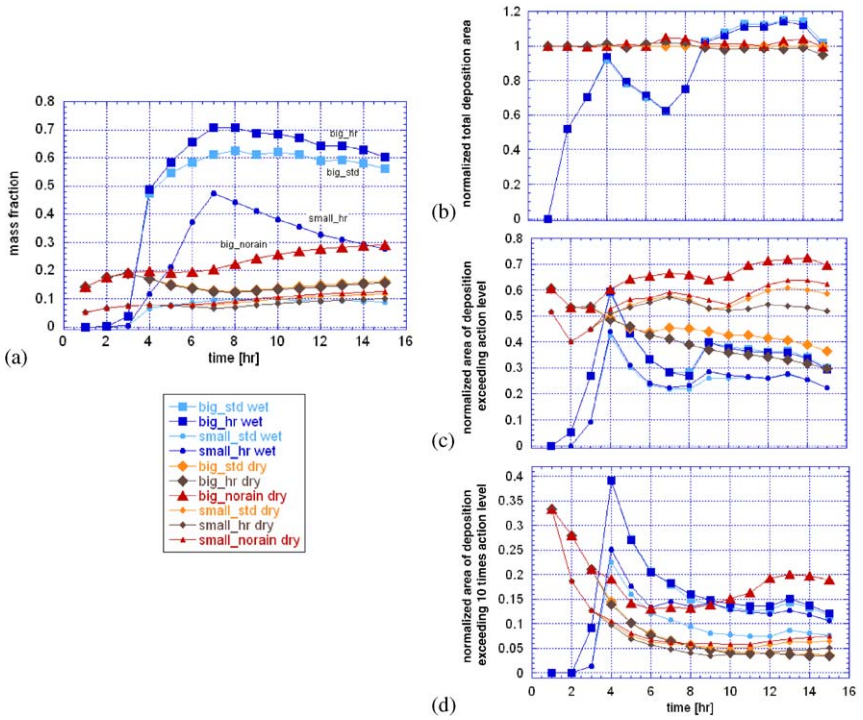

Fig. 6. Comparison of wet and dry deposition (mass, and areal coverage) for different algorithms and particle sizes: (a) fraction of total released aerosol mass deposited (wet or dry) over time; (b) area of deposits (wet or dry) over time; (c) area of deposits (wet or dry) for which the mass per unit area is in excess of a critical "action" level; and (d) area of deposits (wet or dry) for which the mass per unit area is in excess $10\times$ a critical "action" level.

the no-rain simulations show more dry deposition than the simulations with rain. In addition, the standard algorithm produces slightly larger dry deposition fields than does the heavy rain algorithm. The effect is not compensatory, because dry deposition is not as effective as wet deposition for the particle sizes of interest. For example, substantially less mass was deposited (perhaps 20%), wet plus dry, for small_std than for small_hr (35–60%).

At hour 4, when the heavy rain is first evident, and when the rained-on plume fraction is sufficiently high, big_hr and big_std exceed the other mass fractions by more than a factor of two. The small_hr mass fraction lags behind, because so many more of the particles are unaffected by the heavy rain. It is interesting to note that the mass fraction for the small_hr and big_hr cases peaks at hour 7, the most heavy and localized rain event. The increased occurrence of heavy rain appears more important than the reduced plume coverage evident in Fig. 4.

To enable meaningful comparisons between the various deposition fields, an action level (corresponding to a critical dose limit) of 200 Bq kg^{-1} was used for CS-137 deposition (1.6×10^{4} Bq m^{-2}, computed using values of 1.6 for the bulk density and 5 cm for the soil depth (NCRP, 1999)). Three area plots are shown: total area covered (Fig. 6b), area in excess of the action level (Fig. 6c), and area in excess of 10 times the action level (Fig. 6d). All areas are normalized by the area of the no-rain dry deposition field for the big particle size distribution, at the time shown. Table 2 presents the peak values, and the times corresponding to those peaks, for the quantities plotted in Fig. 6. In the total area plot (Fig. 6b), values for small and big simulations are indistinguishable. The area of wet deposition is small until about hour 4, when the rain coverage and heavy rain values become significant. The general shape of the wet deposition curve mimics the shape of the rained-on plume fraction curve presented as Fig. 4a. This similarity simply demonstrates that larger spatial plume coverage by rain provides larger wet deposition areas.

The wet deposition areas finally exceed dry deposition because of an important computational issue; dry deposition is computed only for particles very near the ground (particles are exponentially decayed within a deposition layer of 1 m), whereas wet deposition is computed at all heights if the two-dimensional rain value at that horizontal location is non-zero. Particle size decreases at greater distances from the source, because deposition (dry and wet) removes the larger

Table 2
Peak values from normalized deposited mass and deposition areas shown in Fig. 6

	Simulation and deposition method (wet or dry)	Hour of maximum	Maximum value
Mass fraction (deposited mass normalized by total mass emitted up to that time of the simulation)	big_std wet	8	0.625
	big_hr wet	7.8	0.708
	small_std wet	10	0.097
	small_hr wet	7	0.474
	big_std dry	3	0.189
	big_hr dry	3	0.189
	big_norain dry	15	0.291
	small_std dry	15	0.116
	small_hr dry	15	0.100
	small_norain dry	15	0.125
Normalized total deposit area (deposition normalized by total area of big_norain dry deposit at same time)	big_std wet	13	1.15
	big_hr wet	13	1.14
	small_std wet	13	1.15
	small_hr wet	13	1.14
	big_std dry	(all, by definition)	1.00
	big_hr dry	7	1.02
	big_norain dry	7	1.05
	small_std dry	(all times)	1.00
	small_hr dry	7	1.02
	small_norain dry	7	1.05
Normalized area of deposition in excess of critical action level (deposition normalized by total area of big_norain dry deposit at same time)	big_std wet	4	0.590
	big_hr wet	4	0.596
	small_std wet	4	0.426
	small_hr wet	4	0.441
	big_std dry	1	0.606
	big_hr dry	1	0.606
	big_norain dry	14	0.725
	small_std dry	13	0.609
	small_hr dry	7	0.572
	small_norain dry	13	0.638
Normalized area of deposition in excess of 10 times action level (deposition normalized by total area of big_norain dry deposit at same time)	big_std wet	4	0.391
	big_hr wet	4	0.391
	small_std wet	4	0.226
	small_hr wet	4	0.251
	big_std dry	1	0.333
	big_hr dry	1	0.333
	big_norain dry	1	0.333
	small_std dry	1	0.333
	small_hr dry	1	0.333
	small_norain dry	1	0.333

particles preferentially, allowing at least some of the smaller particles to drift out of the (dry) deposition layer where they are still subject to wet deposition. The sharp drop in rained-on plume coverage at the 15th hour may be responsible for the corresponding drop in wet deposition area at the end of the simulation.

After hour 7, the area of wet deposition exceeding the action level (Fig. 6c) is slightly larger for big_std than big_hr, but the effect is reversed at 10 times the action level (Fig. 6d), because of the concentrating effect of the heavy rain algorithm. This effect is not obvious for the smaller size distribution. The area of wet deposition exceeding the action level for small_std is just slightly smaller than that for small_hr; the area exceeding 10 times the action level for small_std is only 60–70% of that for small_hr. A jump in wet deposition areas in excess of the action level is seen at hour 9, reflective of the increase in rained-on plume fraction. After hour 10, the big_norain dry deposition in excess of 10 times the action level exceeds all of the wet deposition, which likely occurs because the release is continuous; dry deposition continues to be important in these later simulation hours, but the rain is significantly decreased.

In these figures the concentrating effect of wet deposition is evident. Wet deposition provides a smaller area in excess of the action level, than does dry deposition, for most of the simulations (big_hr is an exception), however, the area in excess of 10 times the action level is greater with wet deposition than with dry, even for the small mmd. Similarly, the area in excess of the action level is larger for big_std than for big_hr, which has a greater concentrating effect.

Plots of deposited mass fractions in excess of the action level (and 10 times that level) are not shown because the trends follow the same shape as the total deposited mass fractions (Fig. 6a). The wet deposition fractions in excess of the action level are only slightly smaller than the total deposited mass fractions; the bulk of the deposited mass is in the smaller area. In the dry deposition cases, the differences are only slightly greater, with differences of a few percent between the mass fractions in the total deposition and those greater than 10 times the action level.

5. Summary

We provide an overview of conventional below-cloud scavenging models and suggest a modification for heavy rain events. The algorithms were exercised using a sample multi-sensor rainfall data set. They are shown to predict complex patterns of deposition reflective of locally high precipitation rates. Wet deposition accounts for 10–70% of the material deposited for these simulations. Dry deposition continues to be important, even in the presence of rain.

The heavy rain algorithm provides a credible means for enhancing precipitation scavenging in areas of heavy rain or when there is in-cloud scavenging. Because in-cloud scavenging can also be effective at smaller precipitation rates and in non-convective scenarios, below-cloud scavenging alone may underestimate wet deposition. The effects of the heavy rain algorithm are highly sensitive to the aerosol size distribution. This sensitivity underscores the need for accurate specification of source term size. In-cloud processes increase the particle size distribution above the "Greenfield gap" (Kleinman and Daum, 1991), increasing the scavenging efficiency. Detailed deposition pattern data are needed to validate the algorithms discussed here and provide further information on the physical processes of wet deposition. Advances in remote sensing provide continuous, longer-term monitoring of airborne conditions that would support studies with dense, long-term surface sampling arrays for target study areas.

Acknowledgements

This work was performed under the auspices of the US Department of Energy by University of California Lawrence Livermore National Laboratory under contract No. W-7405-Eng-48. The authors gratefully acknowledge the suggestions of Dr. J. Lundquist and of two anonymous reviewers, which significantly improved the paper.

References

Andronache, C., 2003. Estimated variability of below-cloud aerosol removal by rainfall for observed aerosol size distributions. Atmospheric Chemistry and Physics 3, 131–143.

Carstens, J.C., Martin, J.J., 1982. In-cloud scavenging by thermophoresis, diffusiophoresis, and Brownian diffusion. Journal of the Atmospheric Sciences 39, 1124–1129.

Chate, D.M., et al., 2003. Scavenging of aerosols and their chemical species by rain. Atmospheric Environment 37, 2477–2484.

Chin, H.N.S., 1994. The impact of the ice phase and radiation on a midlatitude squall line system. Journal of the Atmospheric Sciences 51 (22), 3320–3343.

Cunning, J.B., 1986. The Oklahoma–Kansas preliminary regional experiment for STORM-central. Bulletin of the American Meteorological Society 67 (12), 1478–1486.

Daum, P.H., et al., 1990. Measurement and interpretation of concentrations of H_2O_2 and related species in the upper midwest during summer. Journal of Geophysical Research 95 (D7), 9857–9871.

Flossmann, A.I., 1985. A theoretical study of the wet removal of atmospheric pollutants. Part I: the redistribution of aerosol particles captured through nucleation and impaction

scavenging by growing cloud drops. Journal of the Atmospheric Sciences 42, 583–606.

Greenfield, S.M., 1957. Rain scavenging of radioactive particulate matter from the atmosphere. Journal of Meteorology 14, 115–123.

Gudiksen, P.H., Lange, R., 1986. Atmospheric dispersion modeling of radioactivity releases from the Chernobyl Event, LLNL: UCRL-95363, Lawrence Livermore National Laboratory, Livermore.

Horn, H.G., et al., 1988. Collection efficiency of aerosol particles by raindrops. Journal of Aerosol Science 19 (7), 855–858.

Jylha, K., 1991. Empirical scavenging coefficients of radioactive substances released from Chernobyl. Atmospheric Environment 25A (2), 263–270.

Kleinman, L.I., Daum, P.H., 1991. Vertical distribution of aerosol particles, water vapor, and insoluble trace gases in convectively mixed air. Journal of Geophysical Research 96 (D1), 991–1005.

Lawrence, B.A., Shebsovich, M.I., Glaudemans, M.J., Tilles, P.S., 2003. Enhancing precipitation estimation capabilities at National Weather Service Field Offices using multisensor precipitation data mosaics. Proceedings of the ProAMS 19th International Conference on Interactive Information Processing Systems (IIPS) for Meteorology, Oceanography, and Hydrology, Long Beach, paper 15.1.

Nasstrom, J.S., Sugiyama, G., Leone, J.M., Ermak, D.L., 2000. A real-time atmospheric dispersion modeling system. Proceedings of the 11th Joint Conference on the Applications of Air Pollution Meteorology. American Meteorological Society, Long Beach, CA, pp. 84–89.

NCEP, 2003. http: //wwwt.emc.ncep.noaa.gov/mmb/ylin/pcpanl/stage4/.

NCRP, 1999. Recommended screening limits for contaminated surface soil and review of factors relevant to site-specific studies, NCRP Report No. 192, NRCP, Bethesda.

Nieto, P.J.G., Garcia, B.A., Diaz, J.M.F., Brana, M.A.R., 1994. Parametric study of selective removal of atmospheric aerosol by below-cloud scavenging. Atmospheric Environment 28 (14), 2335–2342.

Phillips, C.G., Kaye, S.R., 1999. The influence of the viscous boundary layer on the critical Stokes number for particle impaction near a stagnation point. Journal of Aerosol Science 30 (6), 709–718.

Pruppacher, H.R., Klett, J.D., 1980. Microphysics of Clouds and Precipitation. D. Reidel Publishing, Boston, 714pp.

Rogers, R.R., Zawadzki, I.I., 1979. Rainfall statistics for application to plume rainout models. Atmospheric Environment 13, 279–286.

Seinfeld, J.H., Pandis, S.N., 1998. Atmospheric Chemistry and Physics. Wiley, New York, 1326pp.

Seo, D.J., Breidenbach, J.P., Johnson, E.R., 1999. Real-time estimation of MEAN field bias in radar rainfall data. Journal of Hydrology 223, 131–147.

Slinn, W.G.N., 1974. Precipitation scavenging: some problems, approximate solutions, and suggestions for future research. In: Semonin, R.G., Beadle, R.W. (Eds.), Precipitation Scavenging. TIC-ERDA, Illinois, pp. 1–60.

Slinn, W.G.N., 1984. Precipitation scavenging. In: Randerson, D. (Ed.), Atmospheric Science and Power Production. OSTI, Oak Ridge, pp. 466–532.

Sparmacher, H., Fulber, K., Bonka, H., 1993. Below-cloud scavenging of aerosol particles: particle-bound radionuclides—experimental. Atmospheric Environment 27A (4), 605–618.

Willis, P.T., 1984. Functional fits to some observed drop size distributions and parameterization of rain. Journal of the Atmospheric Sciences 41 (9), 1648–1661.